

# TALES TOLD BY COLOURED TANGLES

DANIEL MOSKOVICH AND AVISHY Y. CARMI

ABSTRACT. Tangle machines are a topologically inspired diagrammatic formalism to describe information flow in networks. This paper begins with an expository account of tangle machines motivated by the problem of describing ‘covariance intersection’ fusion of Gaussian estimators in networks. It then discusses learning tangle machines from data. It concludes with two examples in which tangle machines tell stories of adiabatic quantum computations.

## 1. INTRODUCTION

The Kantian explanation for ‘the unreasonable effectiveness of mathematics in the natural sciences’ is that the patterns which we seek out in nature are those patterns with which we are already familiar as innate categories of perception [31]. When we encounter a new phenomenon, perhaps we first seek to describe this phenomenon in the category of perception most familiar to us. Taken one step further, perhaps human choice of research topics is itself influenced by the scientific language of the day.

The conventional graphical language in computer science is the language of flowcharts, which are labeled directed graphs (*e.g.* [5]). A primary feature of a directed graph is *associativity*, meaning that the following process is unambiguously defined: follow an edge  $e_{ab}$  from  $a$  to  $b$ , then another edge  $e_{bc}$  from  $b$  to  $c$ , and then a third edge  $e_{cd}$  from  $c$  to  $d$ . It means the same thing if we append  $e_{cd}$  to  $e_{ab}e_{bc}$  or if we prepend  $e_{ab}$  to  $e_{bc}e_{cd}$ . The language of flowcharts thus natively describes *sequential* processes, although a *concurrency symbol* may be used within a flowchart to express concurrent computations.

In previous work we proposed a diagrammatic formalism which we call ‘tangle machines’ which elements look similar to the coloured tangle diagrams of low dimensional topology [10, 11, 12, 13, 14]. The fundamental property captured by this formalism is *distributivity*. While associativity is a property of sequentially performed independent processes, distributivity is a property of *fusion*. Namely, if we fuse the same information  $c$  to  $a$  and to  $b$  and then fuse the result together, a process we write as  $(a \triangleright c) \triangleright (b \triangleright c)$ , then the redundant appearance of  $c$  is counted only once towards the final result, namely we obtain  $(a \triangleright b) \triangleright c$ . The same property holds also if  $c$  is fused using a different procedure than the one used for  $a$  and  $b$  and for  $a \triangleright c$  and  $b \triangleright c$ .

We may abstractly consider computation as an information fusion process in which the information content of a computer programme is fused with the information content of an input datum to generate an output. To describe the flow of such information by a tangle machine is to suppress temporal and sequential aspects in favour of the distributive aspect of ‘what is ultimately being fused to what?’. It turns out to be the case that we can describe any Turing machine in this fashion

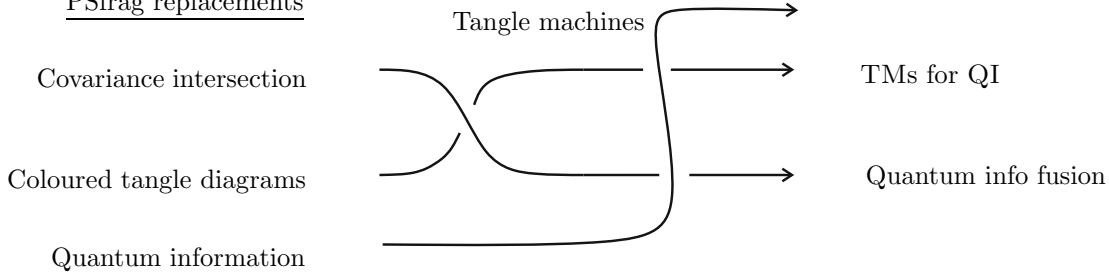


FIGURE 1. A coloured tangle representing this paper.

and if we limit the number of ‘interactions’ then we can describe any computation in the complexity class IP [12]. Parenthetically, we don’t know how much more we can describe by tangle machines— can we describe any computation in complexity class MIP?

A tangle machine tells a tale using something which looks like a diagram of a tangle in low-dimensional topology. The goal of this paper is to introduce tangle machines using fusion of Gaussian estimators as their motivation [10]. We’ll then tell several tales using tangle machines, including one dataset mediating a switch between two other datasets (Section 4), and several adiabatic quantum computations (AQC’s) with different performance features (Section 5).

The organization of this paper is described by the tangle machine of Figure 1. The bottom left arc represents Section 2 in which we discuss a geometric interpretation of fusion of estimators whose joint distribution is unknown. The bottom central arc represents the diagrammatic algebra of low dimensional topology (Section 3.1). Acted on by the bottom left arc, the bottom central arc becomes the central arc, representing the description of information fusion networks by tangle machines (Section 3.2). The above sections represent an expository account of previous published work of the authors.

In Section 4, we discuss the problem of adapting existing causality-detection algorithms to detect tangle machines, and we illustrate by detecting a single crossing in real-world search data.

The bottom right arc, which goes over both of the others, represents quantum probability. Acted on by quantum probability, the bottom left arc becomes the top central arc which represents a geometric description of fusion of random density matrices whose dependence is unknown, not discussed in this paper. The central arc becomes the top right arc, which now represents a tangle machine description of the corresponding notion of a quantum computation. Section 5 presents several examples of adiabatic quantum computations whose flowcharts are represented by tangle machines. A further example may be found in [13, Section 5].

We conclude with a discussion the potential utility of the tangle machine description in Section 6. Tangle machines are revealed to be projections of embedded topological objects, which means that they have *invariants*, that are characteristic quantities giving high-level information about what is happening in the machine [11, 14]. Secondly, tangle machines provide a flexible description, and this flexibility may perhaps be useful for fault tolerance [10].

The father of the use of tangle diagrams as a diagrammatic language for computation is Louis Kauffman, who represented automata, nonstandard set theory, and

lambda calculus with tangle diagrams [27, 28, 8]. Buliga has suggested to represent computations using a different calculus of coloured tangles [7]. In another direction, a different diagrammatic calculus, originating in higher category theory, has been used in the theory of quantum information— see *e.g.* [1, 4, 36]. In all of these approaches an element in a topologically inspired diagrammatic algebra represents a computation and equivalent diagrams represent bisimilar computations. Tangle machines are distinguished by the role of colours, by locality of orientations, and by binding together of operations in ‘interactions’, as discussed in [13].

*Acknowledgement.* D.M. was partially supported by the Helmsley Charitable Trust through the Agricultural, Biological and Cognitive Robotics Initiative of Ben-Gurion University of the Negev.

## 2. AN INFORMATION GEOMETRIC VIEW OF COVARIANCE INTERSECTION

**2.1. Covariance intersection.** Consider a pair of sensors which provide noisy observations about an unknown state vector  $X$ . Each sensor runs its own filtering algorithm to yield an estimate  $X_{1,2}$  of  $X$  and an estimate  $C_{1,2}$  of the error covariance matrix of  $X$ .

$$(2.1) \quad \text{cov} [X - \hat{X}_i] \stackrel{\text{def}}{=} E [(X - \hat{X}_i)(X - \hat{X}_i)^T] \\ - E [X - \hat{X}_i] E [X - \hat{X}_i]^T \quad i = 0, 1, 2 .$$

We wish to optimally integrate these estimates  $(\hat{X}_1, C_1)$  and  $(\hat{X}_2, C_2)$ . It is important that the fused estimate be *consistent* (or *conservative*), meaning that:

$$(2.2) \quad C_i \geq \text{cov} [X - \hat{X}_i] ,$$

*i.e.* that the matrix difference  $C_i - \text{cov} [X - \hat{X}_i]$  is positive semi-definite. We would like all estimators to be consistent because inconsistent estimators may diverge and cause errors.

If the correlations between the estimate errors are known, a linear optimal fusion in the sense of minimum mean estimation error (MMSE) is given by the *Kalman filter*. But such error cross-correlations are typically unknown and may be unmeasurable in real-world settings. Ignoring error cross-correlations can cause the Kalman filter estimates to be non-conservative and perhaps to diverge [15]. The standard approach in applications is to increase the system noise artificially. But proper use of this heuristic requires substantial empirical analysis and compromises the integrity of the Kalman filter framework [33].

*Covariance intersection* provides a method to fuse estimates whose error cross-correlations are unknown in a way that guarantees that the resulting estimate is consistent [26]. The covariance intersection method to fuse estimators  $(\hat{X}_1, C_1)$  with  $(\hat{X}_2, C_2)$  requires a choice of *weight*  $\omega \in (0, 1)$ . The bottleneck for practical covariance intersection is the computation of the optimal value for the weight  $\omega$  with respect to some (typically nonlinear) cost function such as logdet or trace [16, 22]. In the present paper we treat  $\omega$  as a formal parameter or as an unknown constant for each pair of estimates to be fused.

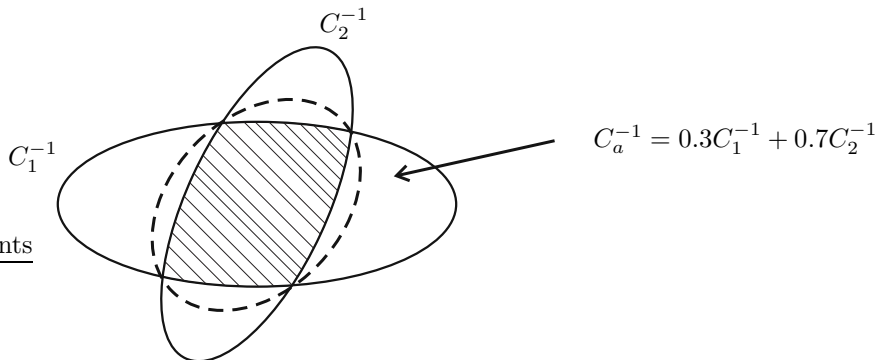


FIGURE 2. The covariance ellipse of the fused estimator is a minimal ellipse that includes within it the intersection of the covariance ellipses of the estimates being fused.

We denote the covariance intersection of  $(\hat{X}_1, C_1)$  with  $(\hat{X}_2, C_2)$  with respect to  $\omega \in (0, 1)$  as follows:

$$(2.3) \quad (\hat{X}_a, C_a)_\omega \stackrel{\text{def}}{=} (\hat{X}_1, C_1) \triangleright_\omega (\hat{X}_2, C_2) .$$

We construct  $(\hat{X}_a, C_a)_\omega$  as follows:

$$(2.4a) \quad \hat{X}_a = (1 - \omega)C_a C_1^{-1} \hat{X}_0 + \omega C_a C_2^{-1} \hat{X}_1 ,$$

$$(2.4b) \quad C_a^{-1} = (1 - \omega)C_1^{-1} + \omega C_2^{-1} .$$

The working principle of covariance intersection is that it fuses two conservative estimates into a third conservative estimate. The reason, for Gaussian estimators, is that the *covariance ellipse* of the fused estimator includes the intersection of the covariance ellipse of the estimators being fused (Figure 2). A *covariance ellipse* of a covariance matrix  $C$  is the locus of vectors  $v$  such that  $v^T C^{-1} v \leq a$  where  $a$  is some arbitrary (but fixed) constant. For Gaussian estimators,  $C^{-1}$  represents the Fisher information. For details see [26].

**2.2. Information geometric interpretation.** Information geometry applies the methods of differential geometry to probability theory [3]. Its main role so far has been to provide geometric coordinate-free elucidation to known facts. The Cramér–Rao inequality, for example, becomes a statement about the statistical manifold changing more in the vicinity of points of high curvature than in the vicinity of points of low curvature.

A *statistical manifold* corresponding to an  $n$ -parameter family of distributions has a point for each possible value of the parameters. Thus, the statistical manifold for all normal distributions over  $\mathbb{R}$  is a surface whose coordinates are  $(\mu, \sigma^2)$ , the order and the variance of the distribution. A statistical manifold has a Riemannian metric called the *Fisher information metric*. With respect to this metric, the statistical manifold of normal distributions is a hyperbolic manifold.

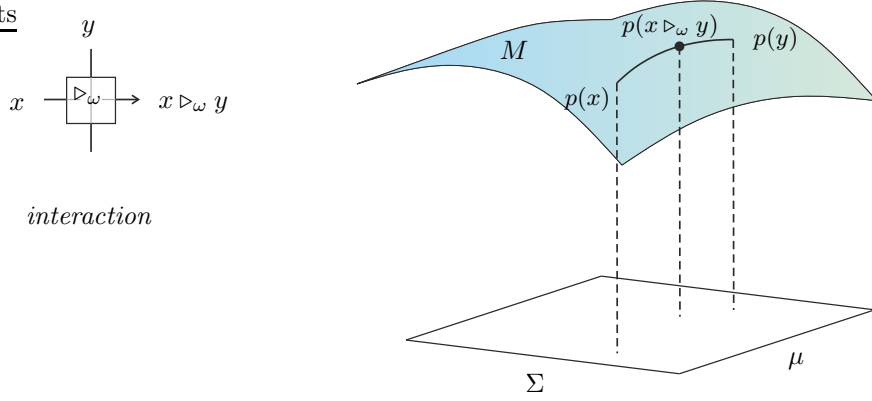


FIGURE 3. A basic information fusion operation (left) and its geometric representation (right). Here,  $p(x)$  denotes a Gaussian distribution with mean  $\hat{X}$  and covariance matrix  $C$ , and thus represents a point in the manifold.

Information geometry provides an interpretation of the 1-parameter family of Gaussian covariance intersections  $\left(\hat{X}_a, C_a\right)_{\omega \in [0,1]}$  as the geodesic from  $\left(\hat{X}_1, C_1\right)$  to  $\left(\hat{X}_2, C_2\right)$ . See Figure 3.

**Proposition 2.1.** *The 1-parameter family of Gaussian covariance intersections  $\left(\hat{X}_a, C_a\right)_{\omega \in [0,1]}$  parameterizes the geodesic from  $\left(\hat{X}_1, C_1\right)$  to  $\left(\hat{X}_2, C_2\right)$ .*

This proposition is proven in the appendix.

**2.3. Properties of covariance intersection.** Covariance intersection has the following properties, which are evident from the geometric interpretation and can also be derived directly from (2.4):

**Idempotence:**

$$a \triangleright_\omega a = a \quad \text{for any estimator } a \text{ and for any } \omega \in (0, 1).$$

**Reversibility:** The function  $\bullet \triangleright_\omega b$  from the statistical manifold to itself is a bijection. Thus, an estimate  $a$  can uniquely be recovered from  $b$ ,  $a \triangleright_\omega b$ , and  $\omega$ .

**No double counting:** For any estimators  $a$ ,  $b$ , and  $c$  and for any weights  $\omega, \omega' \in (0, 1)$ , we have:

$$(2.5) \quad (a \triangleright_{\omega'} b) \triangleright_\omega c = (a \triangleright_\omega c) \triangleright_{\omega'} (b \triangleright_\omega c) .$$

Thus, the redundant appearance of  $c$  in  $a \triangleright_\omega c$  and in  $b \triangleright_\omega c$  counts only once towards the final result. This is the key property of covariance intersection that makes it insensitive to the dependence of different estimators.

### 3. COLOURED TANGLE DIAGRAMS IN LOW DIMENSIONAL TOPOLOGY

This section provides a new strand in our tale. Thus, we shall put aside all that came before, and we shall begin afresh.

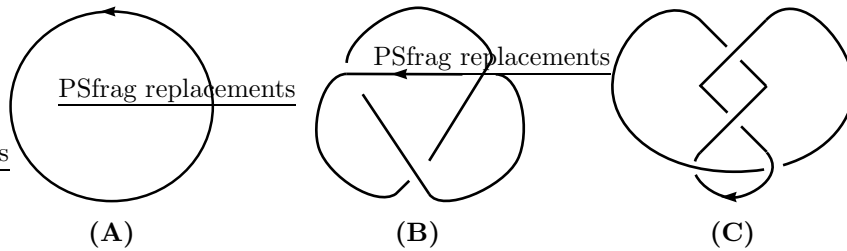


FIGURE 4. The unknot, the trefoil, and the figure-eight knot.

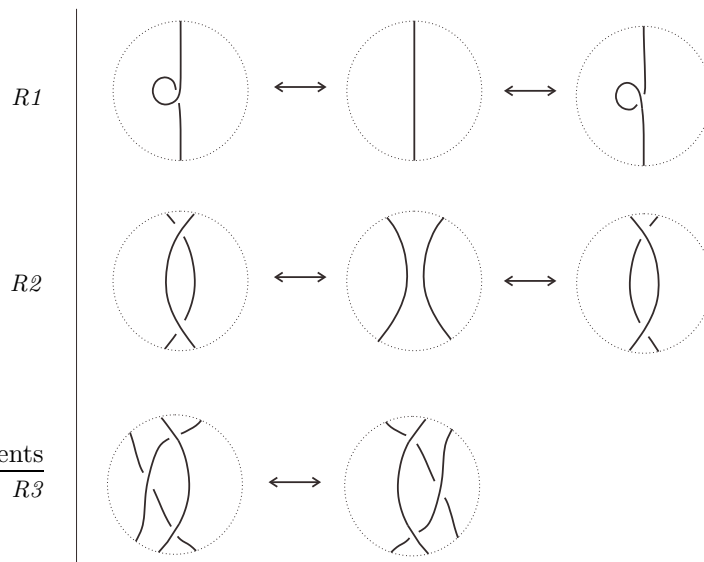


FIGURE 5. The Reidemeister moves. Orientations are arbitrary. To execute a Reidemeister move, cut out a disc inside a tangle diagram containing one of the patterns above, and replace it with another disc containing the pattern on the other side of the Reidemeister move.

**3.1. Colouring knots and tangles.** The fundamental problem in knot theory is to distinguish knots, which are smooth embeddings  $K: S^1 \rightarrow S^3$  of a directed circle into the 3-sphere, considered up to an equivalence relation called *ambient isotopy*. Identifying  $S^3 \simeq \mathbb{R}^3 \cup \{\infty\}$  and choosing a projection of the knot onto a generic plane in  $\mathbb{R}^3$  disjoint from the knot, we may represent  $K$  as a *knot diagram* such as one of those drawn in Figure 4. *Reidemeister's Theorem* tells us that two knot diagrams represent ambient isotopic knots if and only if they are related by a finite sequence of the three *Reidemeister Moves* of Figure 5.

How are we to distinguish two non-ambient-isotopic knots? For example, how are we to distinguish the *trefoil knot* from the *unknot* in Figure 4? The original idea of Tietze [35], as explained later by Fox [21], is to colour each arc in the knot diagram in one of three colours {red, blue, green}, represented numerically as 0, 1, and 2, subject to the constraints that at least two different colours are used, and if two adjacent colours to a crossing are  $i$  and  $j$  then the third adjacent colour is  $i \triangleright j \stackrel{\text{def}}{=} 2i - j \pmod{3}$ .

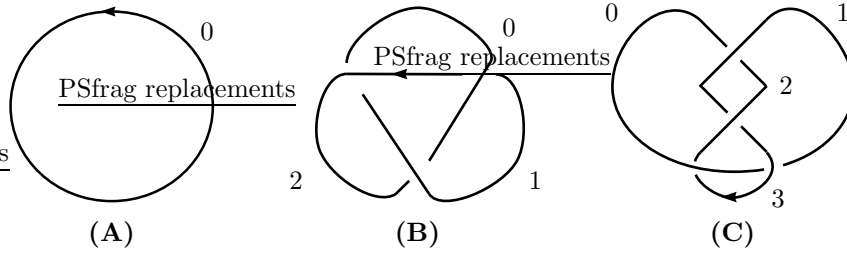


FIGURE 6. A trivial colouring of the unknot, a 3-colouring of the trefoil, and a 5-colouring of the figure-eight knot.

$$(3.1) \quad x \overset{y}{\underset{\downarrow}{-}} x \triangleright y$$

The trefoil can be coloured according to these rules (Figure 6), but the unknot and the figure-eight knot cannot. This property of being 3-colourable is preserved under Reidemeister moves (Figure 12 will later show a more general statement), and thus we have shown that the trefoil is knotted and is not ambient isotopic to the figure-eight knot. But how to show that the figure-eight knot is knotted? Simple. Take five colours 0, 1, 2, 3, and 4, and colour according to the same procedure. The figure-eight knot is 5-colourable, but the trefoil and the unknot are not.

Generalizing, we arrive at the idea of defining an algebraic structure by which a knot can be coloured. Its elements are a set  $Q$  and it comes equipped with an operation  $\triangleright$  satisfying the following axioms:

**Idempotence:**

$$x \triangleright x = x \quad \forall x \in Q .$$

**Automorphism:** The function:

$$\begin{aligned} \triangleright z: Q &\rightarrow Q \\ x &\mapsto x \triangleright z , \end{aligned}$$

is an automorphism of  $(Q, \triangleright)$  for all  $z \in Q$ . In particular it is a bijection of sets and:

$$(3.2) \quad (x \triangleright y) \triangleright z = (x \triangleright z) \triangleright (y \triangleright z) \quad \forall x, y, z \in Q .$$

A structure  $(Q, \triangleright)$  is called a *quandle* (e.g. [25]). Several examples will be given in Section 3.2.

We did not use all of the properties of a knot when defining a quandle colouring. In particular, we did not care about the number of connected components, or whether they were closed. Quandle colourings are defined for *tangles*, that are *concatenations* of crossings, i.e. shapes composed by scattering crossings in the plane and connecting up endpoints via disjoint line segments (Figure 7 shows how a knot diagram can be constructed this way). Actually even planarity plays no role—the connecting segments may intersect transversely. Two tangles are equivalent if they are related by Reidemeister moves. See Figure 8.

We can generalize further. The role of the orientation in the definition of a quandle colouring is to tell us which of the under-arcs of an over-arc coloured  $y$  is



FIGURE 7. A knot formed by concatenating crossings.

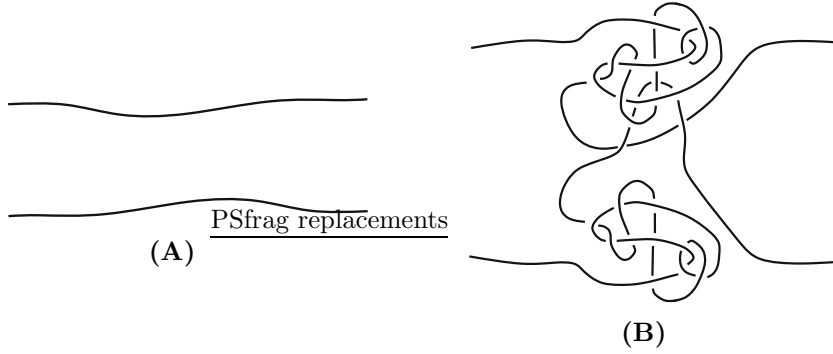


FIGURE 8. Two equivalent tangles.

to be labeled  $x$  and which is to be labeled  $x \triangleright y$ . This is local information and it only plays a role for overcrossing arcs. Moreover there is no reason for directions of overcrossing arcs to match up; a global direction on an arc plays no role.

**3.2. Colouring by information.** The attentive reader will have noticed that the properties of covariance intersection are similar to the quandle axioms, except that there are multiple operations. To bring these under the same roof, let's consider a generalization of a quandle in which  $Q$  is equipped not with one, but with an entire family  $B$  of binary operations, subject to the following axioms:

**Idempotence:**

$$x \triangleright x = x \quad \forall x \in Q \quad \forall \triangleright \in B .$$

**Automorphism:** The function:

$$\begin{aligned} \triangleright z: Q &\rightarrow Q \\ x &\mapsto x \triangleright z , \end{aligned}$$

is an automorphism of  $(Q, B)$  for all  $z \in Q$  and for all  $\triangleright \in B$ . In particular each such function is a bijection of sets, and:

$$(3.3) \quad (x \blacktriangleright y) \triangleright z = (x \triangleright z) \blacktriangleright (y \triangleright z) \quad \forall x, y, z \in Q \quad \forall \triangleright, \blacktriangleright \in B .$$

Such structures, perhaps subject to extra axioms which hold in our cases of interest, are variously called *distributive  $\Gamma$ -idempotent right quasigroups* [6],  *$G$ -family of quandles* [23], and *multi-quandles* [34]. We continue to call them quandles.

We list some examples of quandles:

*Example 3.1* (Conjugation quandle). Colours might be elements of a group  $\Gamma$ , and the operation might be conjugation:

$$(3.4) \quad x \blacktriangleright y \stackrel{\text{def}}{=} y^{-1}xy .$$

The pair  $(\Gamma, \{\blacktriangleright\})$  is called a *conjugation quandle*. If the group  $\Gamma$  is a dihedral group and we colour by reflections, we recover the notion of an  $n$ -colouring of a knot. *e.g.* [21].

*Example 3.2* (Linear quandle). Colours might be elements of a real vector space  $Q$  and the operations might be convex combinations:

$$(3.5) \quad x \triangleright_{\omega} y \stackrel{\text{def}}{=} (1 - \omega)x + \omega y \quad \omega \in D \subseteq \mathbb{R} \setminus \{1\} .$$

The pair  $(Q, \{\triangleright_{\omega}\}_{\omega \in D})$  is called a *linear quandle*.

*Example 3.3* (Loglinear quandle). In the same setting as Example 3.2, consider the operations:

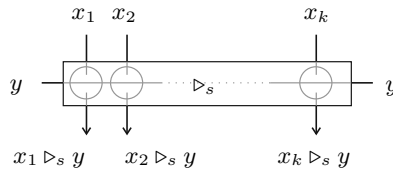
$$(3.6) \quad x \bar{\triangleright}_{\omega} y \stackrel{\text{def}}{=} x^{1-\omega}y^{\omega} \quad \omega \in D \subseteq \mathbb{R} \setminus \{1\} .$$

The pair  $(Q, \{\bar{\triangleright}_{\omega}\}_{\omega \in D})$  is called a *loglinear quandle*.

As we have shown, the set of points of a statistical manifold of Gaussian distributions satisfies the quandle axioms with respect to covariance intersection operations.

There is one further piece of structure to add. The parameter  $\omega$  is an estimated quantity, and in general it will be different for different estimator fusions. When it is the same, we will graphically represent this by thickening the strand. Reidemeister moves  $R2$  and  $R3$  should hold only for thickened strands. We arrive at the recursive definition of a tangle machine.

Our basic building block, which we call an *interaction*, involves one strand coloured  $y$  which we call a *agent* and strands coloured  $x_1, x_2, \dots, x_k$  which we call *patients*. We draw  $y$  as a thick horizontal line, and we label line segments above  $y$  by  $x_1, x_2, \dots, x_k$  correspondingly. An interaction has a weight  $s$  associated to it, and the strands below  $y$  are labeled by  $x_1 \triangleright_s y, x_2 \triangleright_s y, \dots, x_k \triangleright_s y$  correspondingly. We may orient the strand labeled  $y$  or all strands labeled  $x$  (these two conventions are interchangeable). Sometimes we may be sloppy and orient both, in which case the orientations of the patients should be ignored.



Interactions may be concatenated as shown in Figure 9. When labels are estimators, the concatenation of interactions represents a pair of related choices of points on geodesics, as shown in Figure 10.

The lines used for concatenation do not matter, and the equivalence relation on diagrams generated by different choices of concatenating lines, and changes of local orientation, and adding or removing agents where ‘nothing happens’, is illustrated in Figure 11.

Reidemeister moves for machines are illustrated in Figure 12, where the general form of  $R3$  is obtained in Figure 13 where we first replace a box by a thickened line for convenience. We follow this convention for the remainder of the paper.

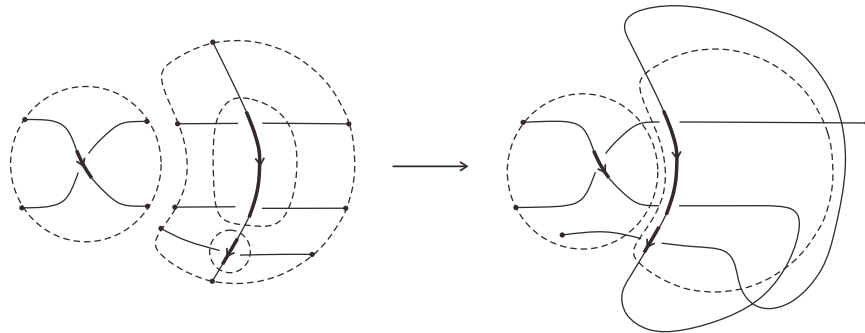


FIGURE 9. Concatenation. Endpoints can be concatenated if they share the same colours (colours are suppressed in the above figure). At the third stage, note that in our formalism, only agents are oriented, and no compatibility requirement is imposed. The concatenation line chosen is arbitrary, and in particular it may intersect other concatenation lines.

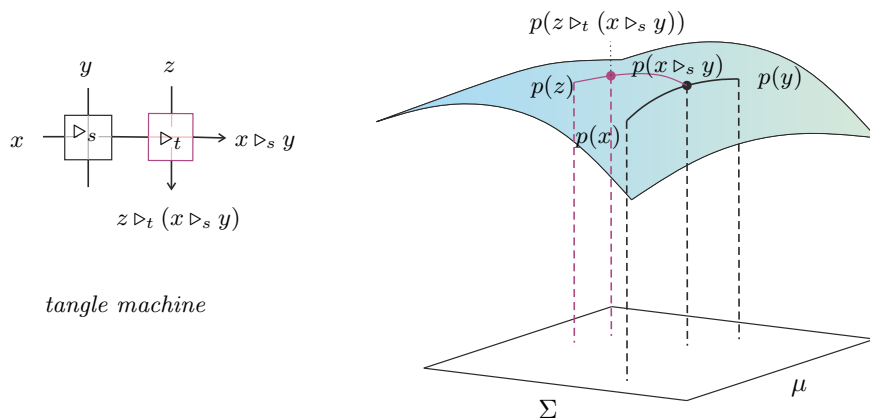


FIGURE 10. An information fusion network – a tangle machine (left) and its geometric representation on a statistical manifold (right).

#### 4. TO LEARN A TANGLE MACHINE

Let's now try a different way to connect tangle machines to the real world. Given a data set we may ask whether there exists a tangle machine which adequately the flow of information such a set. Can a tangle machine represent a data-generating process for real world-data?

In this section we identify an interaction within real world data. It may be possible to expand our method and to adapt existing causality-detection algorithms to construct tangle machines from data.

The idea behind our identification algorithm is that an interaction involving colours  $x$ ,  $y$ , and  $x \triangleright y$ , may be interpreted as a process by which the agent state  $y$  causes the patient to update the old state  $x$  to a new state  $x \triangleright y$ . Suppose we are given three data sets, *e.g.* time-series, associated with  $x$ ,  $y$  and  $x \triangleright y$ . Without knowing the actual identity of each data set, how can we recover the correct causal relationship between them? This is the basic task of recovering an interaction from

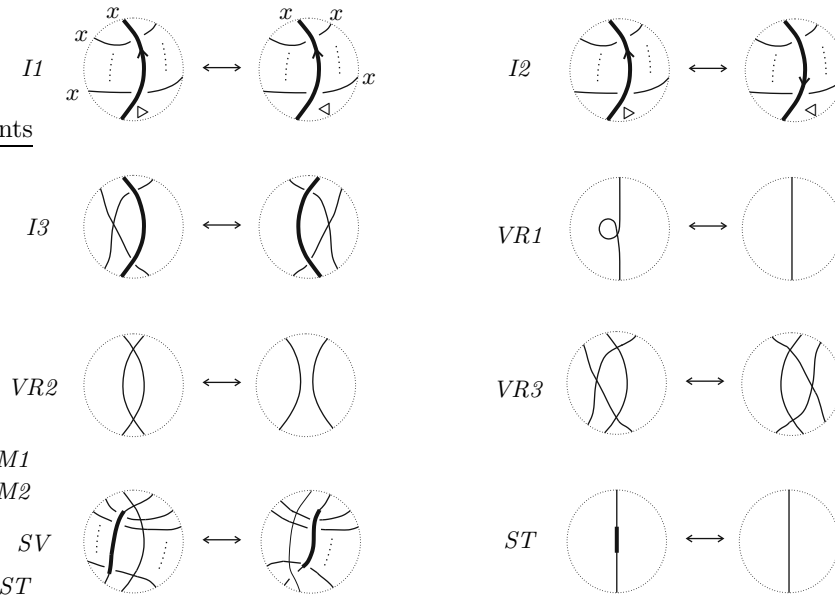


FIGURE 11. Cosmetic moves for machines. Where directions are not indicated, the meaning is that the move is valid for any directions, and the same for colourings.

data. In this simple case we may wish to resort to an analogous Bayesian network whose structure can be discerned using known learning techniques. See Figure 14.

Around 2006, the field of signal processing was revolutionized by the appearance of the concept of *compressed sensing*. Compressed sensing recovers signals using far fewer observations than required by the Shannon–Nyquist sampling theorem. Several people were involved, one of whom was Emmanuel Candes. This story may be described by an interaction of the form: E. Candes *causes* a shift of state from *Shannon–Nyquist sampling* to *compressed sensing*.

We used *Google Trends* to generate time-series data of hits per year from 2000 to 2010 for the three search terms: E. Candes, Shannon–Nyquist sampling, and compressed sensing. We then used the filtering-based detection algorithm described in [9] to recover the underlying Bayesian network. As shown in Figure 15, the actual relationship between the time-series could be recovered up to a time order of Shannon–Nyquist sampling and compressed sensing. There was an ambiguity between two possible interactions both of which identify E. Candes as a cause of the paradigm shift.

We would like to refine and to expand this method to detect machines with more than one interaction.

## 5. TANGLE MACHINES COLOURED BY HAMILTONIANS

**5.1. Tangle machines representing piecewise adiabatic quantum computations.** Quantum information is based on quantum probability theory, in which *density matrices* take the place of classical probability distributions. A set of density matrices may be given the structure of a statistical manifold. A tangent vector

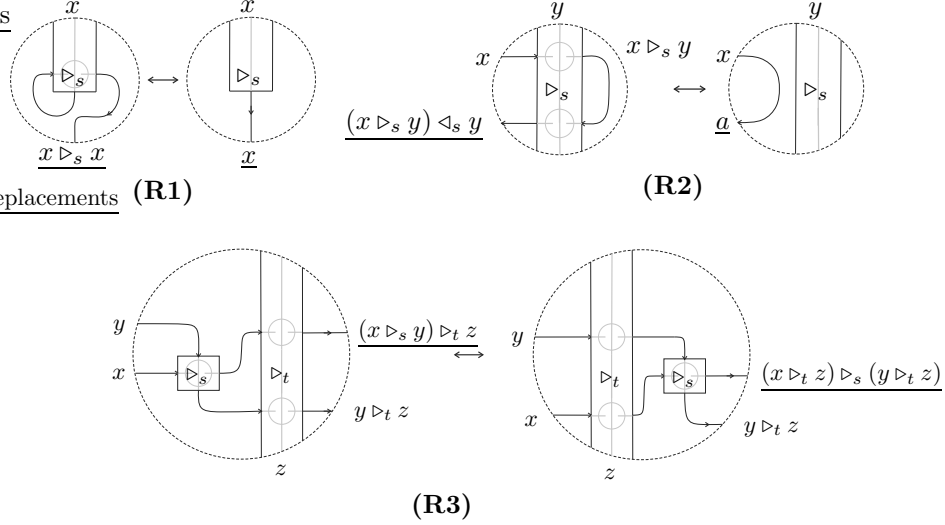


FIGURE 12. The Reidemeister Moves, which are local modifications of information fusion networks. The moves are considered for all orientations on all edges. The properties of information fusion guarantees that the underlined colours on the LHS and on the RHS are equal and thus that these local moves are well-defined. In the R2 move,  $\triangleleft$  represents the implicitly defined inverse operation to  $\triangleright$ . Only a special case of R3 is illustrated above—the general case is given by Figure 13.



FIGURE 13. For simplicity, we draw boxes by thickening the agent. We now draw the general R3 move.

to this manifold is a *Hamiltonian matrix*, which physically describes the dynamics of a quantum system.

One research direction would be to colour tangle machines by density matrices and to fuse them using points on the geodesic between them on the statistical manifold. Instead, we colour our machines by Hamiltonians and we consider the straight line quandle with a time parameter  $s$  that evolves from 0 to 1 [13].

Adiabatic quantum computation (AQC) considers evolving Hamiltonians of the form  $(1 - s)H_0 + sH_1$  to perform quantum computation [18]. Analogously to (2.4) in which the statistical moments of two estimators are fused, the interaction with output:

$$(5.1) \quad H_s = H_0 \triangleright_s H_1 \stackrel{\text{def}}{=} (1 - s)H_0 + sH_1 \text{ ,}$$

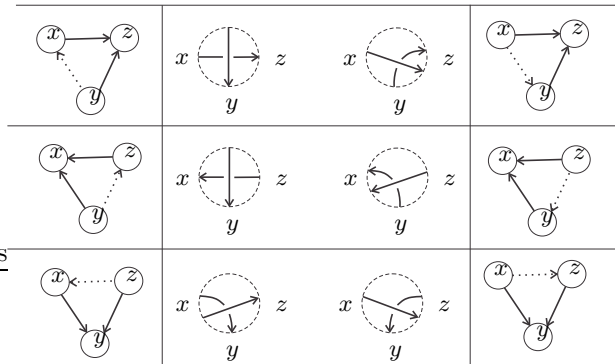


FIGURE 14. Interactions and their Bayesian network analogues. Dashed arrows represent an influence on the patient’s old state. Such influence possibly precedes that which effect the patient’s new state. An interaction-learning algorithm should be able to discerns the correct network configuration.

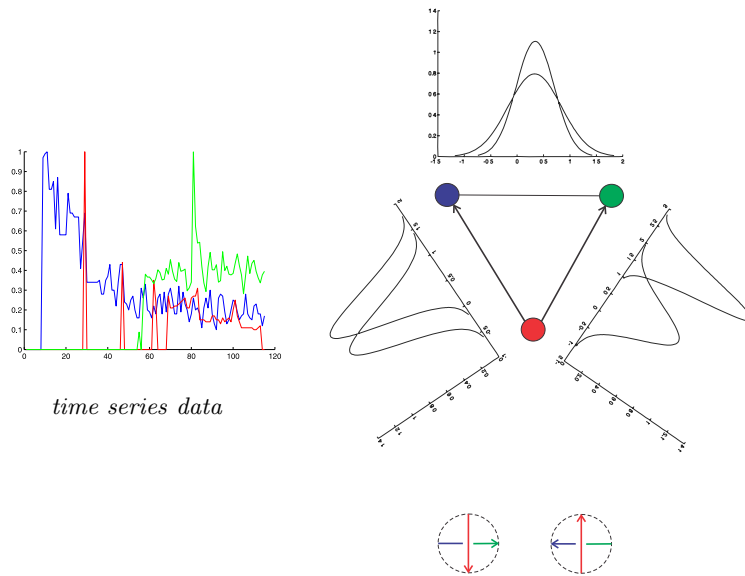


FIGURE 15. Detecting interaction from time-series data. Colour code: Red = E. Candes, Blue = Shannon--Nyquist sampling, Green = compressed sensing. The Bell-curves show the statistical significance of determining the corresponding arrow direction. Roughly, the further apart the curves are for each arrow the more significant is its (causal) direction.

may be viewed as a fusion of two statistical ensembles underlying two quantum systems. As before the parameter  $s \in (0, 1)$  determines the contribution of each component to the new ensemble,  $H_s$ .

The quantum mechanical counterpart of independence of estimators is that the Hamiltonians commute,  $[H_0, H_1] = 0$ , in which case the underlying density matrices

satisfy:

$$(5.2) \quad \rho_s \propto \exp(-\beta H_s) = \exp(-\beta H_0)^{1-s} \exp(-\beta H_1)^s \propto \rho_0^{1-s} \rho_1^s .$$

This is analogous to the formula for a geodesic on a statistical manifold in Section 2.

The idea of AQC is to evolve a Hamiltonian  $H_0$  representing a problem whose solution (the ground state) is easy, into a different and perhaps more complicated Hamiltonian  $H_1$  whose ground state is the solution to the computational task of interest. The computation initializes the system in its ground state, the ground state of  $H_0$ , and then slowly evolves its Hamiltonian to  $H_1$ . This process is called *quantum annealing*. By the Adiabatic Theorem, the system remains in its ground state throughout the evolution process, and the computation concludes at the ground state of  $H_1$ , that is the sought-after solution. The *computing time* of an AQC is inversely proportional to the square of the minimal energy gap between the ground state and the rest of the spectrum, namely to the square of  $g \stackrel{\text{def}}{=}} \lambda_1 - \lambda_0$ , where  $\lambda_{i+1} \geq \lambda_i$  are the underlying energy eigenvalues of the Hamiltonian. Our objective is thus to maximize the minimal  $g$  along the evolution path or to minimize the computation time.

As shown in a previous paper [13] and as we will again illustrate below, a tangle machine may be used to represent a piecewise-defined evolution path of a Hamiltonian. It is well-known that nonlinear evolution paths speed up quantum computation [19, 20]. The topology of the machine itself is only of interest if we can measure its colours at intermediate times and at intermediate arcs. The technological barrier to implementation is the *no-cloning theorem* which tells us that we cannot copy a state, and therefore we have lost it the moment we have measured it. From a future technological perspective we might envision a solution in which concatenation of interactions occurs by means of *quantum teleportation* of an entire Hamiltonian from one interaction to the next. In such a case the tangle machine representation of an AQC would have all of the same features as a tangle machine representation of a classical information fusion network. Without such technology, the tangle machines below merely tell us a tale of Hamiltonian evolution.

We define one additional piece of structure. Choose a *time deformation parameter*  $\alpha \in (0, 1)$  and define the normalized time variables:

$$(5.3) \quad t_i = \min\{1, \alpha^{-i}t\}, \quad i = 0, 1, 2, \dots$$

with  $t \in (0, 1)$ . A time parameter  $t_i$  is associated with the  *$i$ -th time-frame*, and by convention all interactions within this ‘time-frame’ (drawn as a region in the plane) are labeled  $t_i$ . For small  $\alpha$ , the computations in the  $k$ -th time-frame nearly terminate when the computations in the  $k - 1$  frame begin. In the limit  $\alpha \rightarrow 0$  we recover sequential computation.

Our diagrams are drawn along a time axis showing the time-frames. Interactions appearing in a particular time-frame, say the  $k$ -th one, are understood to be executed using the respective time parameter, *i.e.*  $\triangleright_{t_k}$ . In what follows we use the shorthand  $\triangleright_k$  for  $\triangleright_{t_k}$ .

**5.2. Time-Entanglement asymmetry.** In this section we describe a computation involving a single pair of qubits in which a product state evolves into an entangled state. As we shall see, the computation time is proportional to the amount of entanglement.

We begin with a standard adiabatic computation

$$(5.4) \quad O(t) = H_0 \triangleright_0 H_1 \quad ,$$

where the initial and problem Hamiltonians are given by:

$$(5.5a) \quad H_0 = P_x^0 \triangleright_{\oplus} P_x^1 \stackrel{\text{def}}{=} (1-a)(P_x^0 \otimes 1) + a(1 \otimes P_x^1) \quad ;$$

$$(5.5b) \quad H_1 = 1 - \left( \lambda |00\rangle + \sqrt{1-\lambda^2} |11\rangle \right) \left( \lambda |00\rangle + \sqrt{1-\lambda^2} |11\rangle \right)^\dagger \quad ;$$

where  $a, \lambda \in (0, 1)$  are fixed parameters. The *projectors* are defined as:

$$(5.6) \quad P_x^j \stackrel{\text{def}}{=} \frac{1}{2}(1 - (-1)^j X) \quad ,$$

where  $X$  is the Pauli  $X$  matrix. The initial ground state is the product  $|01\rangle_x$  whereas the final ground state is a state (written above in the computational basis  $Z$ ) whose entanglement entropy is

$$S(\lambda) = -\lambda^2 \log(\lambda^2) - (1 - \lambda^2) \log(1 - \lambda^2) \quad .$$

A maximally entangled state is obtained for  $\lambda = \frac{1}{\sqrt{2}}$ .

Figure 16 graphs computation time against an increasing  $\lambda$  for two different values of  $a$ .

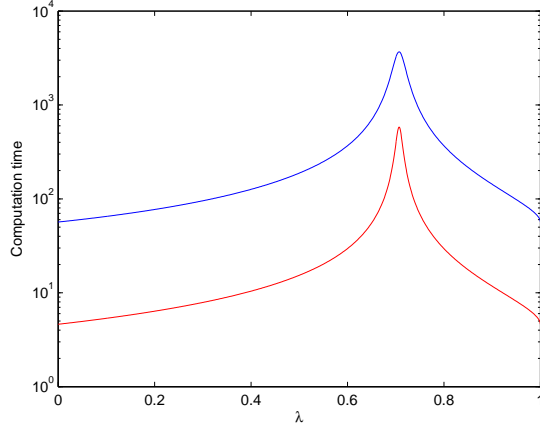


FIGURE 16. Computation time against  $\lambda$  for two values of  $a$ : (Blue)  $a = 0.95$ , and (Red)  $a = 0.5$ .

Let's solve the same problem using a tangle machine and time deformation. We choose time variables as:

$$(5.7) \quad t_1 \stackrel{\text{def}}{=} a \cdot \min\{1, \alpha^{-1}t\}, \quad t_0 = t \quad .$$

Let us solve the same computational problem in two different ways, represented by the tangle machines in Figure 17:

$$(5.8a) \quad O_1(t) = [(P_x^0 \otimes 1) \triangleright_1 (1 \otimes P_x^1)] \triangleright_0 H_1 \quad ;$$

$$(5.8b) \quad O'_1(t) = [(P_x^0 \otimes 1) \triangleright_1 H_1] \triangleright_0 [(1 \otimes P_x^1) \triangleright_1 H_1] \quad .$$

The computation time is graphed with respect to  $\lambda$  in Figure 18. The performance of the standard AQC from Figure 16 is also shown for comparison. Here  $\alpha = 0.5$ .

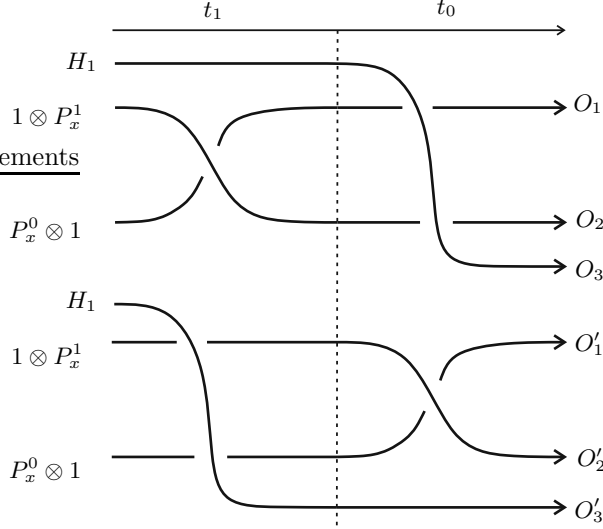


FIGURE 17. Equivalent computations.

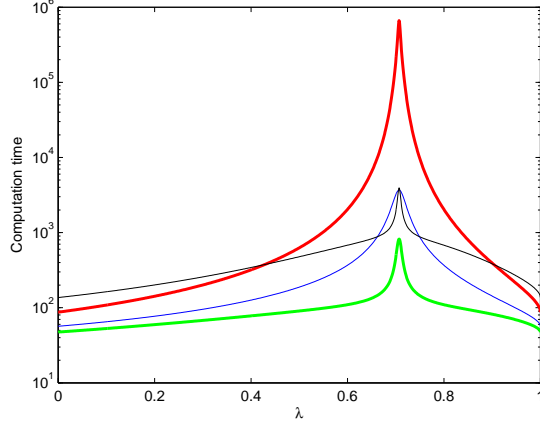


FIGURE 18. Computation time against  $\lambda$  for  $a = 0.95$ . Showing time-deformed AQC (with  $\alpha = 0.5$ )  $O'_1(t)$  (thick red),  $O_1(t)$  (thick green), and standard AQC  $H_0 \triangleright_0 H_1$  (thin blue). The black line corresponds to no time deformation, i.e.  $[(P_x^0 \otimes 1) \triangleright_* (1 \otimes P_x^1)] \triangleright_0 H_1$ , where  $\triangleright_*$  is executed using a time variable  $\min\{a, t_0\}$ .

The difference between the two time-deformed computations,  $O_1(t)$  and  $O'_1(t)$ , is evident. Figure 19 illustrates this further by showing the gap between the computation time of either schemes with respect to  $\lambda$ . We see that the discrepancy between the two computations reaches a peak for a maximally entangled final ground state.

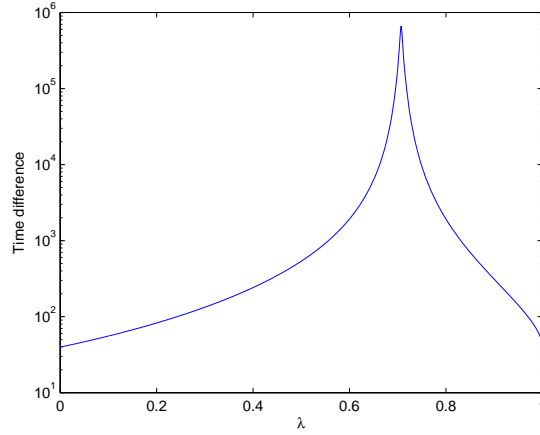


FIGURE 19. Difference in computation time between the two time-deformed computations,  $O_1(t)$  and  $O'_1(t)$ .  $\alpha = 0.5$ .

The performance of the time-deformed algorithms for  $a = 0.5$  and  $\alpha = 0.1$  are shown in Figure 20. This time the computation  $O'_1(t)$  has a clear advantage over  $O_1(t)$  and the standard AQC as the amount of entanglement reaches its peak, around  $\lambda = 1/\sqrt{2}$ .

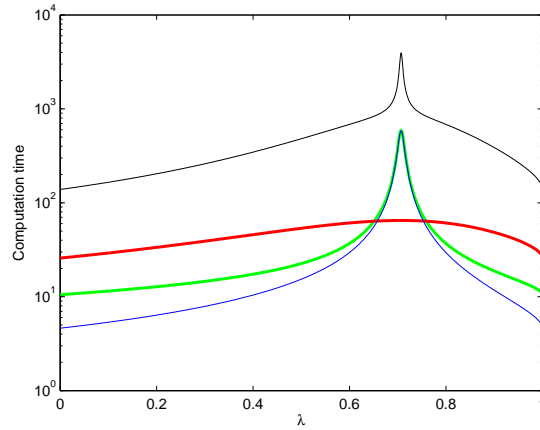


FIGURE 20. Computation time against  $\lambda$  for  $a = 0.5$ . Showing time-deformed AQC (with  $\alpha = 0.1$ )  $O'_1(t)$  (thick red),  $O_1(t)$  (thick green), and standard AQC (thin blue). The black line corresponds to no time deformation, *i.e.*  $[(P_x^0 \otimes 1) \triangleright_* (1 \otimes P_x^1)] \triangleright_0 H_1$ , where  $\triangleright_*$  is executed using a time parameter  $\min\{a, t_0\}$ .

**5.3. 2-SAT example.** In this example we consider a Boolean 2-SAT problem over four variables (qubits). We wish to find a satisfiable assignment for the following

disjunctive normal form (DNF) expression

$$(5.9) \quad ((x_1 \wedge x_2) \vee (\neg x_1 \wedge \neg x_2)) \wedge ((x_3 \wedge x_4) \vee (\neg x_3 \wedge \neg x_4)) .$$

There are four such assignments, namely,  $(0, 0, 0, 0)$ ,  $(0, 0, 1, 1)$ ,  $(1, 1, 0, 0)$ ,  $(1, 1, 1, 1)$ . The final Hamiltonian corresponding to this problem is composed of 2-local Hamiltonians. To see this we define the projector

$$(5.10) \quad P_z \stackrel{\text{def}}{=} \frac{1}{2}(I - Z) ,$$

where  $Z$  is the Pauli  $Z$  matrix. We see that:

$$(5.11) \quad P_z |x\rangle = x |x\rangle , \quad P_z \otimes P_z |xy\rangle = (x \wedge y) |xy\rangle , \quad P_z \oplus P_z |xy\rangle = (x \vee y) |xy\rangle , \quad (1 - P_z) |x\rangle = (\neg x) |x\rangle .$$

An encoding of the above 2-SAT is then given by:

$$(5.12) \quad H_1 = 1 - \frac{1}{2} [P_z^2 + (1 - P_z)^2] \otimes \frac{1}{2} [P_z^2 + (1 - P_z)^2] \\ = 1 - \frac{1}{4} [P_z^4 + P_z^2(1 - P_z)^2 + (1 - P_z)^2 P_z^2 + (1 - P_z)^4] ,$$

where we have used shorthands  $P_z^2$  and  $P_z(1 - P_z)$  for  $P_z \otimes P_z$  and for  $P_z \otimes (1 - P_z)$  respectively.

The problem Hamiltonian has a degenerate ground state whose basis vectors are satisfying assignments for our 2-SAT. Suppose there is an oracle with a probability of  $1/4$  of yielding any one of the four satisfying assignment. This oracle is represented by a black-box Hamiltonian whose ground state is a superposition of the four assignments. Hence,

$$(5.13) \quad H_{\clubsuit} = 1 - |v\rangle \langle v| , \quad |v\rangle = \frac{1}{2} (|0000\rangle + |0011\rangle + |1100\rangle + |1111\rangle) .$$

The initial Hamiltonian has a ground state  $|0000\rangle_x$ , *i.e.* a superposition of  $2^4$  possible assignments. It is given by

$$(5.14) \quad H_0 = P_x^0 \oplus P_x^0 \oplus P_x^0 \oplus P_x^0 .$$

We describe a number of computations which solve the 2-SAT problem using the oracle's knowledge. These computations differ both in the way in which the oracle's "answers" are processed and in their evaluation of the SAT clauses. The details are as follows. In the first round of experiments we assume that  $H_1$  is given to us. In this case we employ two different time-deformed tangle machines, drawn in Figure 21, which represent the following computations:

$$(5.15a) \quad O_1(t) = (H_0 \triangleright_1 H_{\clubsuit}) \triangleright_0 H_1$$

$$(5.15b) \quad O'_1(t) = (H_0 \triangleright_1 H_1) \triangleright_0 (H_{\clubsuit} \triangleright_1 H_1) .$$

In another round of experiments we embed  $H_1$  into the tangle machine. Hence, instead of using the expression for  $H_1$  in (5.12), we consider  $H_1$  to be computed during the evolution of the system. In other words, we let:

$$(5.16) \quad G(t) = [(1 - P_z^4) \triangleright_{\star} (1 - P_z^2(1 - P_z)^2)] \triangleright_{\star} [(1 - (1 - P_z)^2 P_z^2) \triangleright_{\star} (1 - (1 - P_z)^4)] ,$$

where  $a \triangleright_{\star} b \stackrel{\text{def}}{=} (1 - \frac{1}{2}t)a + \frac{1}{2}tb$ . Note that indeed

$$\lim_{t \rightarrow 1} G(t) = H_1 .$$

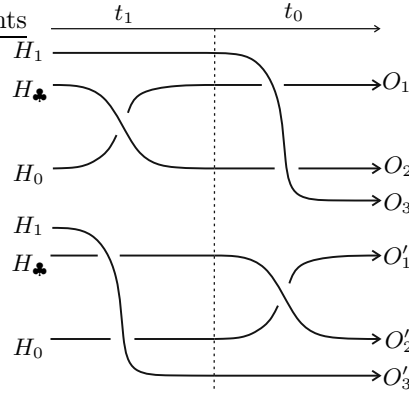


FIGURE 21. Equivalent computations.

Substituting  $H_1$  with its evolving version  $G(t)$  in (5.15) yields

$$(5.17a) \quad O_1(t) = (H_0 \triangleright_1 H_{\clubsuit}) \triangleright_0 G(t)$$

$$(5.17b) \quad O'_1(t) = (H_0 \triangleright_1 G(t)) \triangleright_0 (H_{\clubsuit} \triangleright_1 G(t)) .$$

The diagrams describing the two computations are shown in Figure 22. The dashed region represents the logic underlying  $G(t)$ . Note that the number of inputs/outputs of this *submachine* corresponds to the number of conjunctive clauses in the original DNF (5.9).

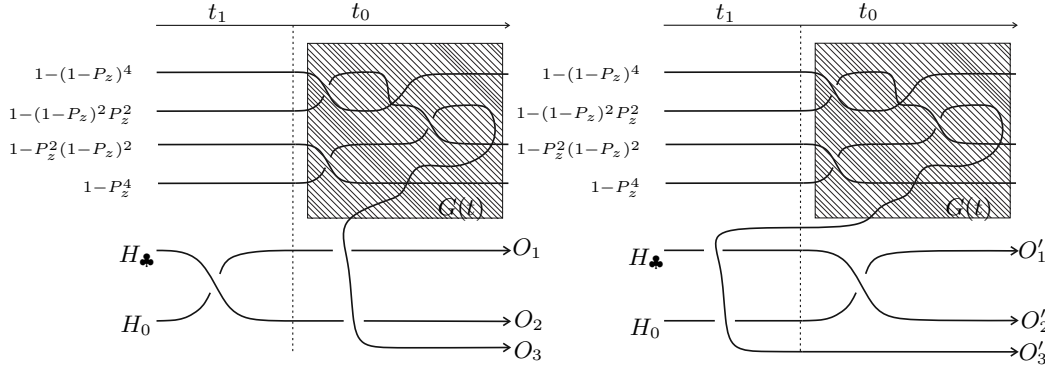


FIGURE 22. Equivalent computations in which the problem Hamiltonian logic is encoded within the tangle (dashed region).

Figure 23 shows the energy gap over time for the various modes of computation in this example. Here we use  $\alpha = 0.5$ .

## 6. UTILITY OF TANGLE MACHINES

In this paper we have introduced tangle machines and they have told us tales of information flow in networks in both classical and quantum settings. In what way can this distributive structure be of use to information theorists and to computer scientists? We present two advantages that such a topological description provides following [14] and [10].

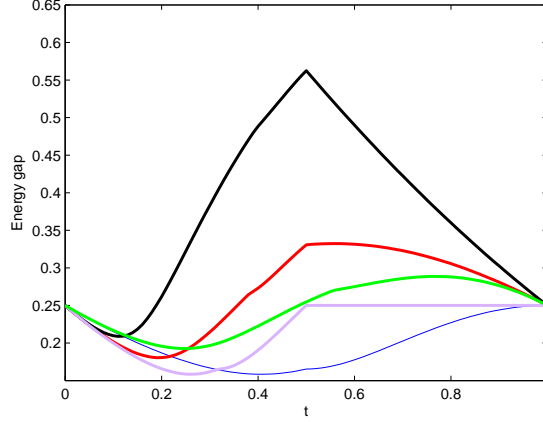


FIGURE 23. Energy gaps in the qudit example. Standard AQC using  $H_1$  (thin blue), standard AQC using  $G(t)$  (green), time-deformed AQC using  $H_1$  (purple), time-deformed AQC  $O_1(t)$  using  $G(t)$  (red), time-deformed AQC  $O'_1(t)$  using  $G(t)$  (black).

**6.1. Topological invariants.** Knot diagrams are planar projections of knots in  $\mathbb{R}^3$  equipped with over/under information. Knots in 3-space are ambient isotopic if and only if any two diagrams that represent them are related by a finite sequence of Reidemeister moves. Is there an analogous topological interpretation for tangle machines?

We have shown that tangle machines arise as planar projections of objects we call *inca foams* [14], that are necklaces of spheres glued together along disjoint discs, all jointly embedded in  $\mathbb{R}^4$ . Two inca foams are ambient isotopic if and only if any two tangle machines which represent them are related by a finite sequence of Reidemeister moves. This topological interpretation provides us tools to construct and to study *topological invariants* of tangle machines, that are characteristic quantities which coincide when tangle machines are equivalent. These will ideally have clear and compelling interpretations in terms of information. We mention two invariants.

**Shannon capacity:** There is a well-defined notion of *Shannon capacity* for a graph which measures the Shannon capacity of an communications channel defined by the graph (*e.g.* [17]). This notion extends to tangle machines [14].

Define an assignment of colours to arcs of a tangle machine  $M$  to be *confusable* if there is one of these colours that is uniquely determined by the others. Let  $\text{Cap}_k(M)$  denote the number of distinct assignments of  $k$  colours to arcs of  $M$  which  $M$  admits. Now define:

$$(6.1) \quad \text{Cap}(M) \stackrel{\text{def}}{=} \sup_{k \in \mathbb{N}} \sqrt[k]{\text{Cap}_k(M)}$$

**Complexity:** Knots admit a binary operation called *connect sum* under which they form a commutative monoid:

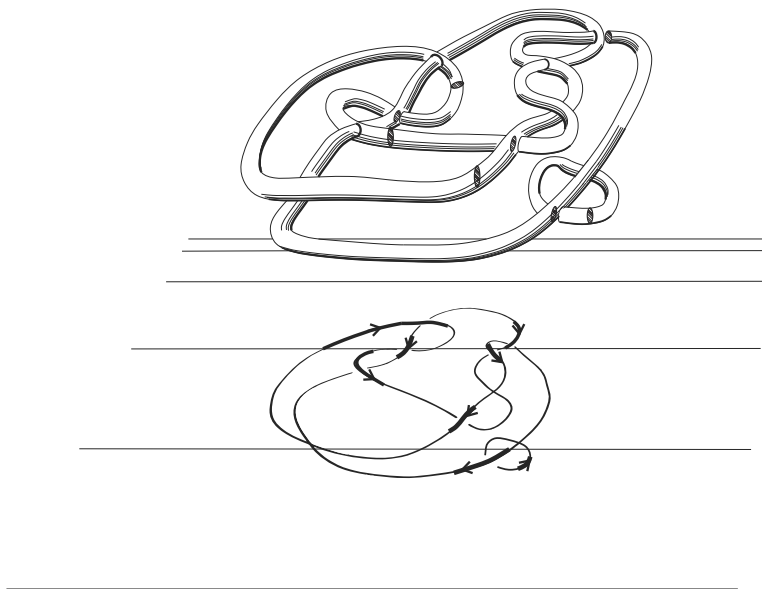


FIGURE 24. An Inca foam and a tangle machine representing it.

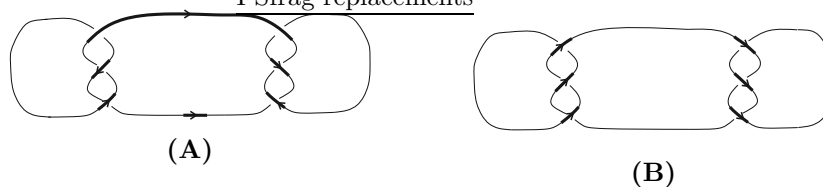
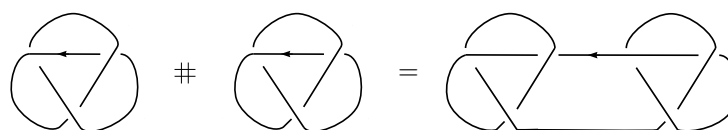


FIGURE 25. Machine 25A has complexity 1. Machine 25B has complexity 2 if the horizontal strands are the same colour, otherwise it too has complexity 1.



Coloured knots also form a commutative monoid under the connect-sum operation [32]. Although many related diagrammatic algebraic structures do not [29, 30], tangle machines also form a commutative monoid under the connect-sum operation [14]. More generally, we may define two sub-machines as being *independent* if they are connected along a set of arcs all of which share the same colour [11]. The maximal number of nontrivial connect-summands is a topological invariant of tangle machines, and is a (rough) measure of tangle machine complexity. See Figure 25.

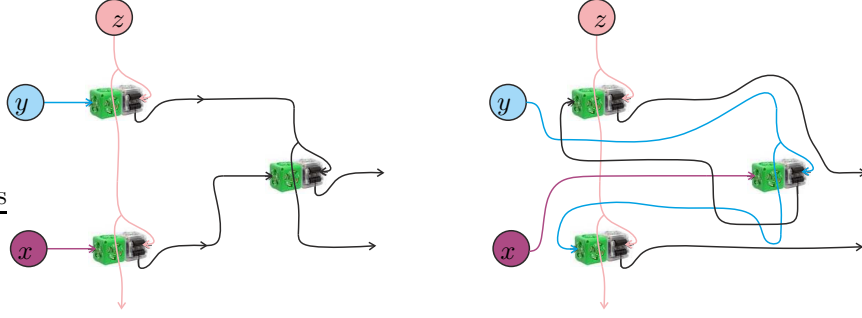


FIGURE 26. The R3 move realized using cubelets. Both these networks have the same outputs and thus represent different realizations of essentially the same modular robot. The cubelets themselves do not move, and what changes is only the configuration of which cubelet sends its output to which other cubelet.

**6.2. Flexibility of description.** A second advantage of the tangle machine formalism is that, unlike directed graphs, it is flexible. Reidemeister moves give different machines representing different information flows which globally achieve the same task.

In Section 5 we will give examples in which the performance of one machine is significantly better than the performance of an equivalent machine although both achieve the same task. Further examples are in [13]. Here, following [10], we shall present an idea for an application of the tangle machine description to fault tolerance of sensor networks which perform fusion using covariance intersection.

We may imagine a realization of a tangle machine using with modular robots called ‘cubelets’ as shown in Figure 26. See [www.modrobotics.com/cubelets/](http://www.modrobotics.com/cubelets/).

Three transmitting devices continuously stream data  $x(T)$ ,  $y(T)$ , and  $z(T)$ . Our task is to combine these data streams, eliminating redundancy (*e.g.* because of the Problem of Double Counting [24]). Two schemes to combine the data streams at a fixed time  $T \geq 0$  are represented by the left and the right hand side of the R3 move in Figure 12.

In the left machine, combine  $x(T)$  and  $y(T)$  with  $z(T)$  with parameter  $t \in (0, 1)$  to obtain fused data streams  $x(T) \triangleright_t z(T)$  and  $y(T) \triangleright_t z(T)$ . Assume that all estimators are Gaussian and that the fusion is performed using covariance intersection. We read the fusion from bottom to top because the overcrossing arc is directed from left to right. If it were oriented from right to left, we would read from top to bottom and we would be filtering out the data stream  $z(T)$  from  $x(T) \triangleright_t z(T)$  and from  $y(T) \triangleright_t z(T)$ . On the right,  $x(T) \triangleright_t z(T)$  is combined with  $y(T) \triangleright_t z(T)$  using a weight  $s \in (0, 1)$ .

The left and the right machine describe equivalent data stream fusion schemes, which is visually indicated by the fact that the diagrams are related by sliding one overcrossing arc over another. Indeed, the result of the data stream fusion in the right machine is  $(x(T) \triangleright_s y(T)) \triangleright_t z(T)$ , which is the same combined data stream as in the left machine because redundant double appearance of  $z(T)$  in  $x(T) \triangleright_t z(T)$  and  $y(T) \triangleright_t z(T)$  is eliminated by  $\triangleright_s$  by assumption.

However, there is an important difference between these two schemes on the left and right of the R3 move. Imagine at some time  $T_1 > 0$  that stream  $y$  becomes

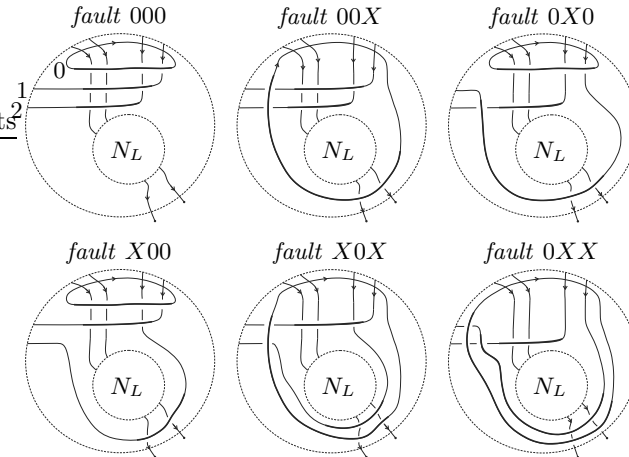


FIGURE 27. Topological fault-tolerance. Switching between equivalent networks ameliorate the effects of faults. The fault code appearing above each network should be read as follows. The digits from left to right correspond to edges 2,1 and 0. An “X” in the place of the  $i$ th digit signifies faulty content in its respective edge.

faulty. In this case the left machine is superior because it contains the intermediate data stream  $x(T) \triangleright_t z(T)$  which might be useful even when  $(x(T) \triangleright_t z(T)) \triangleright_s (y(T) \triangleright_t z(T))$  is junk. Conversely, if  $z$  becomes faulty at some time  $T_2 > 0$  then the right machine would be preferred. The top overcrossing arc might slide back and forth at different times. Thus the machines involved in the R3 move might be describing the underlying logic of a simple fault-tolerant data stream fusion network.

A more general version of the same scheme is described in Figure 27. Consider the network illustrated in the upper left corner of Figure 27. This network has a set of outputs outside the bounding disk (not shown). Some set of intermediate edges lies inside the subnetwork designated by  $N_L$  and represented as an empty circle. In the course of network operation, erroneous streams of data cause one or more of the edges 0,1, and 2, to carry faulty pieces of information, *e.g.* biased, inconsistent and otherwise unreliable estimates. This is detected inside the network. To inhibit the influence of this contamination on edges within  $N_L$ , the network performs Reidemeister moves on itself, transforming itself into an equivalent network. This is achieved by ‘sliding’ the faulty edges all the way over  $N_L$ , by repeated application of the second and third Reidemeister moves. In the resulting topology, the faulty edges have no effect on  $N_L$ , and so local costs are improved.

In the above example, things were as easy as sliding faulty edges forward, but this is only because the networks we considered are topologically uninteresting. In the general case an optimal configuration may be difficult to identify.

REFERENCES

1. Abramsky S. & Coecke, B. 2009 Categorical quantum mechanics. In *Handbook of Quantum Logic and Quantum Structures*, Vol. 2, 261–323. [arXiv:0808.1023](https://arxiv.org/abs/0808.1023)

2. Aharonov, D. & Van Dam, W. & Kempe, J. & Landau, Z. & Lloyd, S. & Regev, O. 2008 Adiabatic Quantum Computation Is Equivalent to Standard Quantum Computation. *SIAM Review* **50**(4), 755–787.
3. Amari, S. & Nagaoka, H. 2007 Methods of information geometry. Translations of Mathematical Monographs (Vol. 191), American Mathematical Soc.
4. Baez, J. & Stay, M. 2011 Physics, topology, logic and computation: A Rosetta stone. In *New Structures for Physics*, Lecture Notes in Phys. **813**, 95–172. [arXiv:0903.0340](#)
5. Bohl, M. & Rynn, M. 2007 Tools for Structured and Object-Oriented Design. Prentice Hall, Upper Saddle River, NJ, USA.
6. Buliga, M. 2011 Braided spaces with dilations and sub-riemannian symmetric spaces. In *Geometry. Exploratory Workshop on Differential Geometry and its Applications*, (D. Andrica & S. Moroianu Ed.), Cluj-Napoca 21–35. [arXiv:1005.5031](#)
7. Buliga, M. 2011 Computing with space: A tangle formalism for chora and difference. Preprint. [arXiv:1103.6007](#)
8. Buliga, M. & Kauffman, L. 2013 GLC actors, artificial chemical connectomes, topological issues and knots. In *ALIFE 14: Proceedings of the Fourteenth International Conference on the Synthesis and Simulation of Living Systems*, 490–497. [arXiv:1312.4333](#)
9. Carmi, A. 2013 Compressive system identification: sequential methods and entropy bounds. *Digit. Signal Process.* **23**(3), 751–770.
10. Carmi, A.Y. & Moskovich, D. 2014 Low dimensional topology for information fusion. In *BICT14: Proceedings of the 8th International Conference on Bio-inspired Information and Communications Technologies*, ACM/EAI, 251–258. [arXiv:1409.5505](#)
11. Carmi, A.Y. & Moskovich, D. 2014 Tangle Machines **II**: Invariants. [arXiv:1404.2863](#)
12. Carmi, A.Y. & Moskovich, D. 2015 Computing with coloured tangles. *Symmetry* **7**(3), 1289–1332. [arXiv:1408.2685](#)
13. Carmi, A.Y. & Moskovich, D. 2015 Tangle machines. *Proc. R. Soc. A* **471**, 20150111. Conference version: Calude, C.S., Dinneen, M.J. (eds.) UCNC 2015, LNCS, vol. 9252, 277– 289. Springer, Heidelberg. [arXiv:1404.2862](#)
14. Carmi, A.Y. & Moskovich, D. 2015 Inca foams. [arXiv:1509.01284](#)
15. Chang, K.C., Chong, C.-Y. & Mori, S. 2010 Analytical and Computational Evaluation of Scalable Distributed Fusion Algorithms. *IEEE Transactions on Aerospace and Electronic Systems* **46**(4), 2022–2034.
16. Chen, L. & Arambel, P.O. & Mehra, R.K. 2002 Estimation under unknown correlation: Covariance intersection revisited. *IEEE T. Automat. Contr.* **47**(11), 1879–1882.
17. Erickson, M.J. 2014 Introduction to Combinatorics. Discrete Mathematics and Optimization **78** (2nd ed.). John Wiley & Sons.
18. Farhi, E. & Goldstone, J. & Gutmann, S. & Sipser, M. 2000 Quantum computation by adiabatic evolution. [arXiv:quant-ph/0001106](#)
19. Farhi, E. & Goldstone, J. & Gutmann, S. 2002 Quantum adiabatic evolution algorithms with different paths. [arXiv:quant-ph/0208135](#)
20. Farhi, E. & Goldstone, J. & Gosset, D. & Gutmann, S. & Meyer, H.B. & Shor, P. 2011 Quantum Adiabatic Algorithms, Small Gaps, and Different Paths. *Quantum Information & Computation* **11**(3–4), 181–214. [arXiv:0909.4766](#)
21. Fox, R.H. 1961 A quick trip through knot theory. in: *Topology of 3-Manifolds and Related Topics*, M.K. Fort (Ed.), Prentice-Hall, NJ, 120–167.
22. Franken, D. & Hupper, A. 2005 Improved fast covariance intersection for distributed data fusion. In *Proceedings of the 8th International Conference on Information Fusion*.
23. Ishii, A., Iwakiri, M., Jang, Y. & Oshiro, K. 2013 A  $G$ -family of quandles and handlebody-knots. *Illinois J. Math.*, **57** 817–838. [arXiv:1205.1855](#)
24. Jazwinski, A.H. 1970 Stochastic Processes and Filtering Theory. New York: Academic Press.
25. Joyce, D. 1982 A classifying invariant of knots: The knot quandle. *J. Pure Appl. Algebra* **23**, 37–65.
26. Julier, S. Uhlmann, J.K. 2001 General decentralized data fusion with covariance intersection. In *Handbook of Multisensor Data Fusion*, CRC Press, Boca Raton, FL.
27. Kauffman, L.H. 1994 Knot automata. In *Twenty-Fourth International Symposium on Multiple-Valued Logic, Conference Proceedings*, May 25-27 1994, Boston, Massachusetts, IEEE Computer Society Press, 328–333.

28. Kauffman, L.H. 1995 Knot logic. In *Knots and Applications* (ed L. Kauffman), Series of Knots and Everything **6**, World Scientific Publications, 1–110.
29. S.G. Kim, Virtual knot groups and their peripheral structure, *J. Knot Theory Ramifications* **9**(6) (2000) 797–812.
30. T. Kishino and S. Satoh, A note on non-classical virtual knots, *J. Knot Theory Ramifications* **13**(7) (2004) 845–856.
31. Knuth, K.H. 2015 The Deeper Roles of Mathematics in Physical Laws. Third place, FQXi essay contest: “2015 Trick or Truth: The mysterious connection between physics and mathematics.” Retrieved from [http://fqxi.org/data/essay-contest-files/Knuth\\_knuth---fqxi-essay---.pdf](http://fqxi.org/data/essay-contest-files/Knuth_knuth---fqxi-essay---.pdf)
32. Moskovich, D. 2006 Surgery untying of coloured knots. *Algebr. Geom. Topol.* **6**, 673–697. [arXiv:math.GT/0506541](https://arxiv.org/abs/math/0506541)
33. Niehsen, W. 2002 Information fusion based on fast covariance intersection filtering. in *Proceedings of the Fifth International Conference on Information Fusion, 2002* **2**(2), 901–904.
34. Przytycki, J.H. 2011 Distributivity versus associativity in the homology theory of algebraic structures. *Demonstration Mathematica* **44**(4), 823–869. [arXiv:1109.4850](https://arxiv.org/abs/1109.4850)
35. Tietze, H.F.F. 1908 Über die topologische Invarianten mehrdimensionaler Mannigfaltigkeiten. *Monatshefte für Mathematik und Physik* **19** 1–118.
36. Vicary, J. 2012 Higher Semantics for Quantum Protocols. In *Proceedings of the 27th Annual ACM/IEEE Symposium on Logic in Computer Science*, 606–615. [arXiv:1207.4563](https://arxiv.org/abs/1207.4563)

APPENDIX

The proof of Proposition 2.1 is the combination of the following two lemmas which are surely well-known.

**Lemma 1.** *The covariance intersection of weight  $\omega \in [0, 1]$  of two unnormalized Gaussian probability density functions  $p(X)$  and  $p(Y)$  is  $p(X)^{1-\omega}p(Y)^\omega$ .*

*Proof.* Let  $p(X), p(Y)$  be unnormalized Gaussian densities parameterized by their mean and covariance,  $(\hat{X}, C_X)$  and  $(\hat{Y}, C_Y)$ , respectively. The pdf  $p(X)^{1-\omega}p(Y)^\omega$  is given by the expression:

$$(2) \quad \exp \left( -\frac{1}{2} \left[ (1-\omega)(Z - \hat{X})^T C_X^{-1} (Z - \hat{X}) + \omega(Z - \hat{Y})^T C_Y^{-1} (Z - \hat{Y}) \right] \right) .$$

We verify that this expression equals:

$$(3) \quad \exp \left( -\frac{1}{2} (Z - \hat{Z})^T C_Z^{-1} (Z - \hat{Z}) \right) ,$$

for:

$$(4a) \quad \hat{Z} = (1-\omega)C_Z C_X^{-1} \hat{X} + \omega C_Z C_Y^{-1} \hat{Y}$$

$$(4b) \quad C_Z^{-1} = (1-\omega)C_X^{-1} + \omega C_Y^{-1} .$$

We compute that  $C_X^{-1} = -\frac{\partial^2 \log p(x)}{\partial x \partial x^T}$  which is called the *precision matrix* of  $p(X)$ . In particular,

$$(5) \quad C_Z^{-1} = -\frac{\partial^2 \log p(z)}{\partial z \partial z^T} = (1-\omega) C_x^{-1} + \omega C_Y^{-1} ,$$

which follows from (.2).

The mode  $\hat{X}$  satisfies:

$$(6) \quad \left. \frac{\partial \log p(x)}{\partial x} \right|_{x=\hat{X}} = 0 .$$

The mode  $\hat{Z}$  of  $p(Z)$  is thus obtained from (.2) by

$$(.7) \quad 2 \left. \frac{\partial \log p(z)}{\partial z} \right|_{z=\hat{Z}} = (1 - \omega) C_x^{-1} (\hat{Z} - \hat{X}) + \omega C_Y^{-1} (\hat{Z} - \hat{Y}) = 0 ,$$

finally giving

$$(.8) \quad C_z^{-1} \hat{Z} = (1 - \omega) C_x^{-1} \hat{X} + \omega C_Y^{-1} \hat{Y} .$$

□

**Lemma .2.** *Let  $P$  be a space of probability density functions (pdfs) over some domain. Consider the functional  $J: P \rightarrow \mathbb{R}$  defined by*

$$(.9) \quad J(g(X)) \stackrel{\text{def}}{=} (1 - \omega) \text{KL}(g(X) \| p(X)) + \omega \text{KL}(g(X) \| q(X))$$

where  $g(X)$ ,  $p(X)$ , and  $q(X)$  are pdfs in  $P$  and  $\text{KL}(\cdot \| \cdot)$  is the Kullback–Leibler divergence. Then the following holds for any  $\omega \in [0, 1]$  and  $g(X) \in P$ :

$$J \left( \frac{p(x)^{1-\omega} q(x)^\omega}{\int_x p(x)^{1-\omega} q(x)^\omega dx} \right) \leq J(g(X)) .$$

*Proof.* Writing down the Kullback–Leibler divergence explicitly, we have:

$$(.10) \quad \begin{aligned} \min_{g(X)} J(g(X)) &= \min_{g(X)} \left[ (1 - \omega) \int_x g(x) \log \frac{g(x)}{p(x)} dx + \omega \int_x g(x) \log \frac{g(x)}{q(x)} dx \right] = \\ &= \min_{g(X)} \int_x g(x) \log \frac{g(x)}{p(x)^{1-\omega} q(x)^\omega} dx = \\ &= \min_{g(X)} \left[ \int_x g(x) \log \frac{g(x)}{p(x)^{1-\omega} q(x)^\omega} dx + \int_x p(x)^{1-\omega} q(x)^\omega dx - \int_x p(x)^{1-\omega} q(x)^\omega dx \right] = \\ &= \min_{g(X)} \left[ \text{KL} \left( g(X) \left\| \frac{p(X)^{1-\omega} q(X)^\omega}{\int_x p(x)^{1-\omega} q(x)^\omega dx} \right. \right) \right] - \int_x p(x)^{1-\omega} q(x)^\omega dx . \end{aligned}$$

But  $\text{KL}(\cdot \| \cdot) \geq 0$  vanishes if and only if its arguments coincide, and the result follows. □